Review of Scientific Instruments ARTICLE scitation.org/journal/rsi

A simplified cryogenic optical resonator apparatus providing ultra-low frequency drift

Cite as: Rev. Sci. Instrum. 91, 045112 (2020); doi: 10.1063/1.5140321
Submitted: 26 November 2019 • Accepted: 2 April 2020 •
Published Online: 17 April 2020

Eugen Wiens,[1] Chang Jian Kwong,[1] Timo Müller,[2] and Stephan Schiller[1,a)]

AFFILIATIONS

[1]Institut für Experimentalphysik, Heinrich-Heine-Universität Düsseldorf, 40225 Düsseldorf, Germany
[2]Siltronic AG, Johannes-Hess-Straße 24, 84489 Burghausen, Germany

[a)]Author to whom correspondence should be addressed: step.schiller@hhu.de

ABSTRACT

A system providing an optical frequency with instability comparable to that of a hydrogen maser is presented. It consists of a 5 cm long, vertically oriented silicon optical resonator operated at temperatures between 1.5 K and 3.6 K in a closed-cycle cryostat with a low-temperature Joule–Thomson stage. We show that with a standard cryostat, a simple cryogenic optomechanical setup, and no active or passive vibration isolation, a minimum frequency instability of 2.5×10^{-15} at $\tau = 1500$ s integration time can be reached. The influence of pulse-tube vibrations was minimized by using a resonator designed for low acceleration sensitivity. With reduced optical laser power and interrogation duty cycle, an ultra-low fractional frequency drift of -2.6×10^{-19}/s is reached. At 3.5 K, the resonator frequency exhibits a vanishing thermal sensitivity and an ultra-small temperature derivative $8.5 \times 10^{-12}/\mathrm{K}^2$. These are favorable properties that should lead to high performance also in simpler cryostats not equipped with a Joule–Thomson stage.

I. INTRODUCTION

Optical resonators play an important role in the generation of laser light with ultra-stable frequency. They are essential to the field of optical atomic clocks, where they are utilized for the pre-stabilization of the laser wave used for the interrogation of ultra-narrow atomic transitions.[1–3] Other applications are in gravitational wave detectors[4,5] and for tests of fundamental physics.[6–11]

The most common type of resonator consists of a hollow spacer of length L, which introduces a fixed separation between two mirrors that are optically contacted to its end surfaces. The design of the spacer geometry and support is usually optimized to reduce length variations produced by environmental vibrations. To counteract thermally induced variations in length, the resonators are usually made of materials that exhibit a particularly low thermal expansion coefficient at the desired operational temperature. Ultra-low-expansion (ULE) glass is today the most common material for use at or near room temperature. Another promising material is the ceramic Nexcera.[12–14] However, the Brownian motion imposes a fundamental limitation to their length stability.[15] This is on the order of 1×10^{-15} for room-temperature resonators with a typical length of ≤10 cm.[16–20] The instability was successfully lowered to 8×10^{-17} using a 48 cm long resonator.[21] Furthermore, room-temperature resonators made of the ULE material suffer from drift. The drift rates vary substantially between units, with one of the smallest values being 1.6×10^{-17}/s.[14] One approach for reducing both limitations is the operation of the resonators at cryogenic temperatures.[6,7,22–29]

Here, we present a cryogenic single-crystal silicon resonator developed for low vibration sensitivity and frequency stability comparable to that of a hydrogen maser, operated in a cryogenic system of moderate complexity. In order to reduce the resonator manufacturing cost, we simplified the design to a cylindrical shape. A fairly complete characterization of the resonator was possible using a system composed of a stable interrogation laser, a frequency comb, and a hydrogen maser.

II. DESIGN

A. Cryostat accelerations

The goal of our resonator design was to minimize its acceleration sensitivity in order to achieve good performance in

closed-cycle cryostats that provide no advanced vibration isolation. In such units, the pulse-tube and seismic accelerations are transmitted to the optical setup. As an example, our closed-cycle cryostat (Leiden Cryogenics, CF-1K) exhibits the acceleration spectrum displayed in Fig. 1(a). The accelerations were measured on the optical setup, during operation at 1.5 K, for the three cartesian axes using a precise interferometric sensor. With an optical head of the sensor located outside the cryostat, we used optical windows to reflect a laser beam from the device under test. While it is best to measure the acceleration directly on the resonator, here, this was possible only for its vertical motion, because of the limited optical access. To measure this motion, the laser interferometer beam was reflected from one of its end faces. The motion along the two horizontal directions was instead measured by reflecting the sensing laser beams from two other silicon resonators (designated as "Si1" and "Si2") contained within the cryostat.

The spectrum consists of peaks at multiples of 1.4 Hz, the base frequency of the pulse-tube cooler. The total acceleration integrated over the frequency range from 1 Hz to 200 Hz is 4.9×10^{-3} g [see Fig. 1(b)]. The largest contribution arises from the vibrations introduced by the rotary valve stepper motor, which operates with a frequency close to 150 Hz. Contribution from the vibrations of the lab ground, measured with a high-sensitivity piezoelectric transducer, is shown in Figs. 1(c) and 1(d) and is on the order of 0.9×10^{-3} g. It is dominated by the vertical component.

Because of this high acceleration level (compared to a standard room-temperature setup placed on a standard active vibration isolation platform), a minimized acceleration sensitivity of the resonator frequency is clearly necessary.

B. FEM simulations

The resonator developed in this work is a vertically oriented, axially symmetric structure, supported at three points. It follows the concept presented in Refs. 22–24, 26, and 27 but was further simplified by avoiding the conical spacer shape and employing instead a simple cylindrical shape. The spacer diameter and length were chosen to be 37 mm and L = 50 mm, respectively; the mirror substrates are of standard one-inch diameter and 6.3 mm thick. All the other geometry parameters were optimized using a commercial finite-element-method (FEM) package (Ansys). The optical axis of the resonator was aligned with the [111] crystallographic direction of the silicon crystal, which is the direction with the highest Young's modulus. We used the silicon stiffness matrix from Ref. 30 in our simulation. The optimization was done by calculating the acceleration sensitivity of the resonator, defined as fractional length change per unit acceleration, $\Delta L/(a_i\, L)$, for different values of the geometrical parameters and for different directions i of the acceleration. After defining a set of values, we studied the influence of imprecise optical contacting, of an offset of the resonator's position relative to the

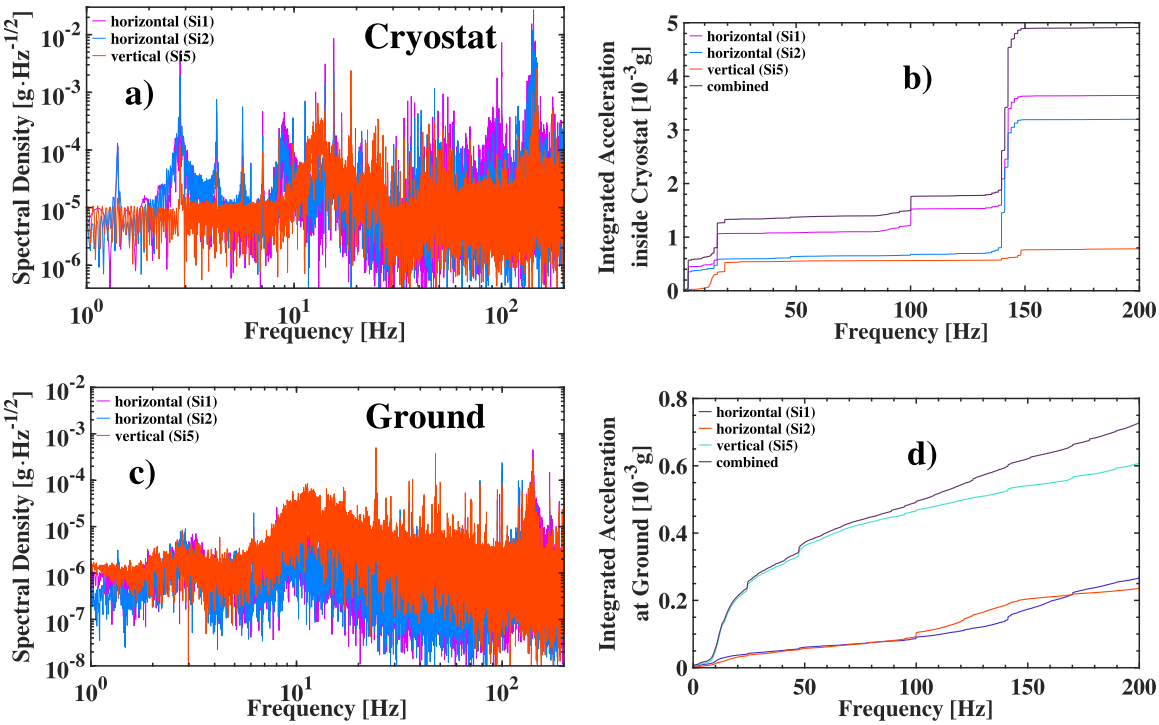

FIG. 1. Acceleration measured at three experimental plates inside the operating cryostat and ground acceleration. [(a) and (c)] Spectral density of acceleration $S_{a,i}(f)$, i = x, y, z, in the three spatial directions. The red curve in panel (a) indicates the level measured on the plate that supports the 5 cm resonator described in this work. [(b) and (d)] The total accelerations $\left[\int_0^f (S_{a,i}(f'))^2 df'\right]^{1/2}$. The combined total acceleration is the root sum-of-squares of the three individual total accelerations.

three support points (fixed in space), and of manufacturing tolerance (assumed to be 0.1 mm). Our optimization was aimed at minimization of these three sensitivities. This resulted in a support ring with diameter and thickness of 67 mm and 20 mm, respectively, an offset of the ring from the horizontal center plane toward the top of 0.51 mm, and a diameter of the central bore of 15 mm. The venting hole has 2 mm diameter, is located in the upper half of the resonator, is centered 5 mm below the top surface, and forms an angle of 63° with the [100] crystallographic direction of the silicon crystal. Partial results of the sensitivity calculations are displayed in Figs. 2(a)–2(c).

With three supports placed at a radial distance of 26 mm from the optical axis of the resonator, the acceleration sensitivity variation with a vertical offset of the support ring, under 1 g vertical acceleration, is $16 \times 10^{-11}/(g\ \text{mm})$. The sensitivity to an imperfect radial positioning of the resonator relative to the supports is $5 \times 10^{-11}/(g\ \text{mm})$, and the sensitivity to a parallel offset of the optical axis from the symmetry axis of the resonator is $4 \times 10^{-11}/(g\ \text{mm})$.

We also simulated the effect of rotation of the resonator around the vertical symmetry axis, while the support points remained fixed in space. The result is presented in Fig. 2(d). It resembles closely

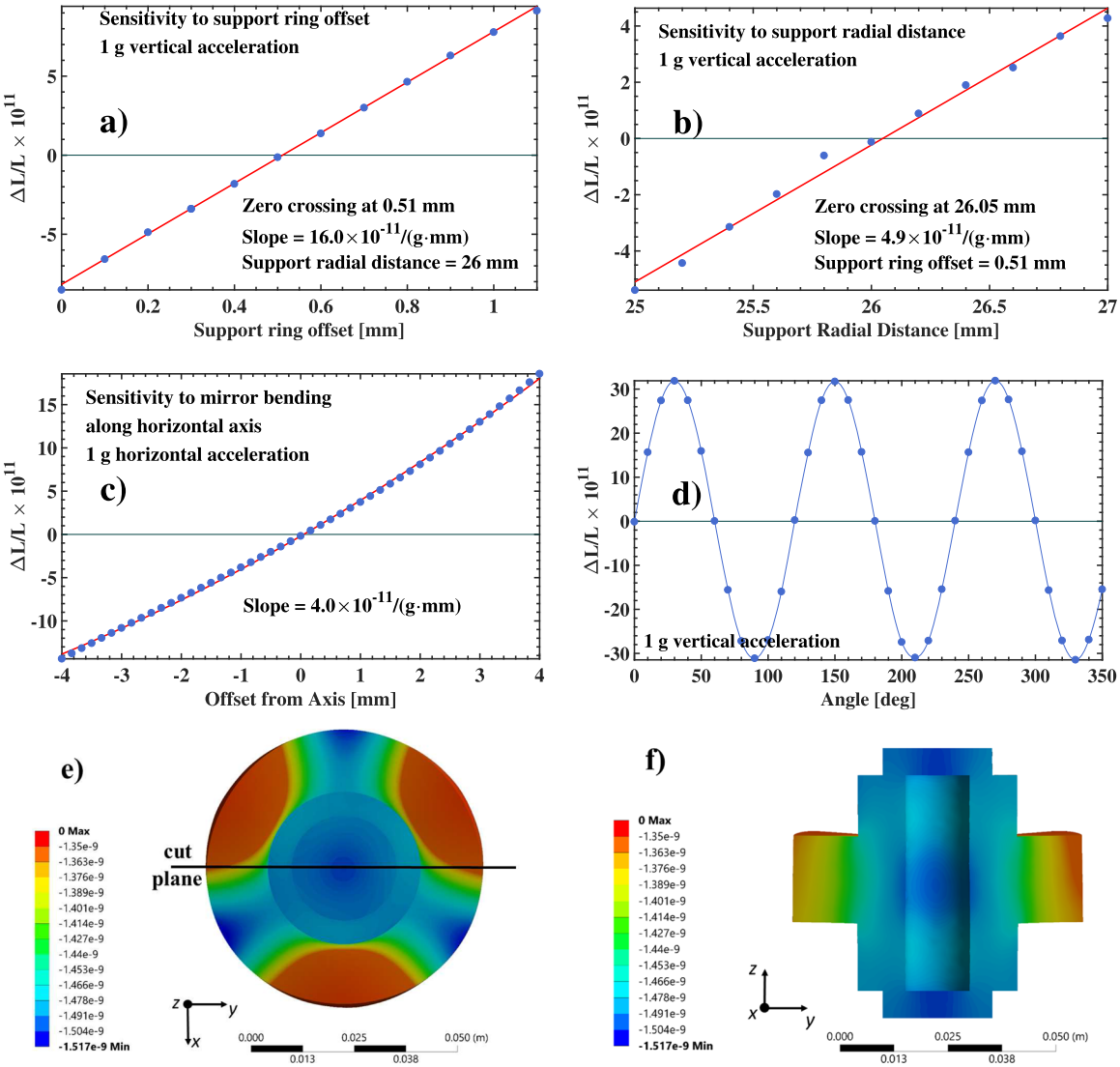

FIG. 2. Acceleration sensitivities of the resonator according to FEM simulations. (a) Influence of the imperfect manufacturing of the support ring on sensitivity during an application of 1 g vertical acceleration. (b) Sensitivity to changes in the radial position of the three supports and 1 g vertical acceleration. (c) Sensitivity to the offset of the optical axis from the symmetry axis of the resonator (1 g acceleration is applied in the transverse direction). (d) Sensitivity to rotation of the resonator around the symmetry axis and an application of 1 g vertical acceleration. [(e) and (f)] Examples of the simulation results for the resonator with optimized shape. Color indicates the displacement in meter along the vertical direction (z-axis) due to the application of 1 g vertical acceleration. In (e), the displacement of the surfaces is shown; in (f), the displacements of the volume elements in the midplane cut along the vertical YZ plane [see the definition of the cut plane in (e)] are shown.

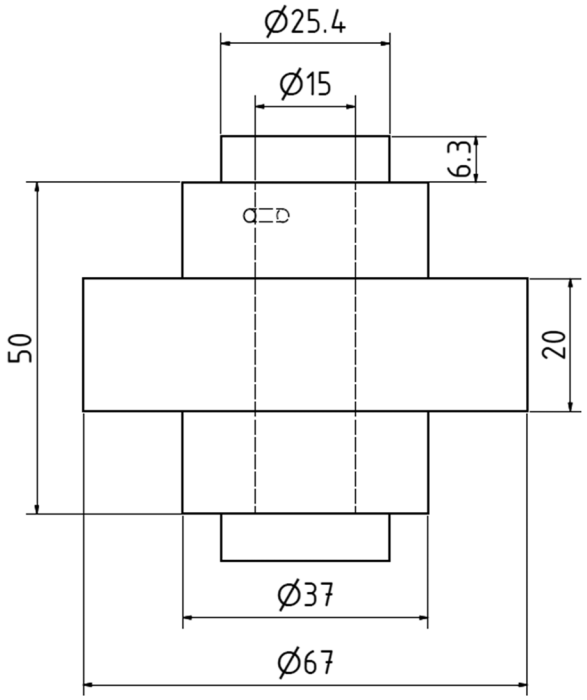

FIG. 3. Optimized design of the resonator, as determined using FEM simulations. The 2 mm diameter venting hole is located in the upper half at a distance of 5 mm from the top end. Dimensions are in mm.

the result obtained by Matei *et al.*[31] The sensitivity is periodic with a period of 120° due to silicon's anisotropic crystal structure and has an amplitude of $3 \times 10^{-10}/g$. This results in a slope of $5 \times 10^{-12}/(g \text{ deg})$ around the sensitivity's zero crossing.

Figures 2(e) and 2(f) display the deformation of the resonator of optimum shape (without manufacturing errors), which is placed on the three supports at the optimum position, with resultant zero sensitivities. In the simulation, vertically oriented 1 g acceleration is applied to all volume elements. The simulation reveals a displacement of the top and bottom mirrors by the same amount, approximately 1.5 nm, leaving the distance between them, and thus, the resonator frequency unchanged. The final geometry of the resonator after FEM optimization is presented in Fig. 3.

C. Modeling of thermal noise

Random Brownian movement of the atoms in the crystal lattice of the spacer and of the substrates as well as in the mirror coatings results in a random fluctuation of the distance between the mirror internal surfaces.[15] Thus, this motion directly influences the optical path length and sets fundamental limits to the frequency stability of a laser wave whose frequency is locked to the resonator. For future reference, we calculate the thermal-noise induced instability of the resonator length at 1.5 K, assuming the parameters listed in Table I. The results are presented in Table II. A 13-fold reduction in thermal noise from 300 K to 1.5 K is predicted to the level 2.8×10^{-17} at 1.5 K. The coating contributes over 96% to the total noise, because of its amorphous nature. The use of crystalline mirrors could here provide a significant further reduction. In the present work, the performance of the system is not limited by the thermal noise.

TABLE I. Parameters used for the calculation of thermal noise.

Symbol	Parameter	Value
λ	Laser light wavelength	1562 nm
L	Length of the spacer	50 mm
R_{sp}	Radius of the spacer	18.5 mm
r_b	Radius of the central bore	7.5 mm
$w_{R=1m}$	Beam waist at the curved mirror	338 μm
$w_{R=\infty}$	Beam waist at the flat mirror	329 μm
E	Young's modulus of Si along the [111] crystallographic direction[32]	187.9 GPa
ν	Poisson's ratio of Si along the [111] crystallographic direction[32]	0.18
$Q_{Si} = 1/\phi_{Si}$	Si quality factor[33]	10^8
ϕ_{ct}	Coating loss factor[34]	1 mrad
d_{ct}	Coating thickness	9.38 μm

TABLE II. Computed fractional frequency instability of the mirror distance due to Brownian noise for different operating temperatures. The contributions from the spacer, the substrates, and the coatings are given. The parameters of Table I were assumed. The fractional frequency instability is expressed as an Allan deviation σ_y, which is independent of integration time.

	σ_y (10^{-17})				
Temperature (K)	300	124	16.8	4	1.5
Spacer	0.21	0.13	0.05	0.02	0.01
Substrates	1.31	0.84	0.3	0.15	0.09
Coatings	39.0	25.1	9.2	4.5	2.8
Total	39.0	25.1	9.2	4.5	2.8

III. APPARATUS

A. Resonator and resonator support

The resonator (denoted by "Si5" in some figures) was manufactured from a cylindrical silicon crystal (resistivity 8 kΩ/cm and diameter 4 in.), grown along the [111] crystallographic direction using the float zone method. The optical axis of the resonator is aligned with this direction. The two end faces were polished to optical quality. High-reflectivity dielectric mirrors for 1.5 μm wavelength were optically contacted to them in-house. These silicon substrates originate from a different block of material, having a resistivity of 4 kΩ/cm and a diameter of 4 in. Their symmetry axes are oriented along the [100] crystallographic direction. This aspect was not included in the above simulations.

The resonator was installed in an optical setup inside a pulse-tube cryostat equipped with a Joule–Thomson stage (Leiden Cryogenics). A picture of the setup and the corresponding schematic are shown in Fig. 4. The resonator was supported from below at three

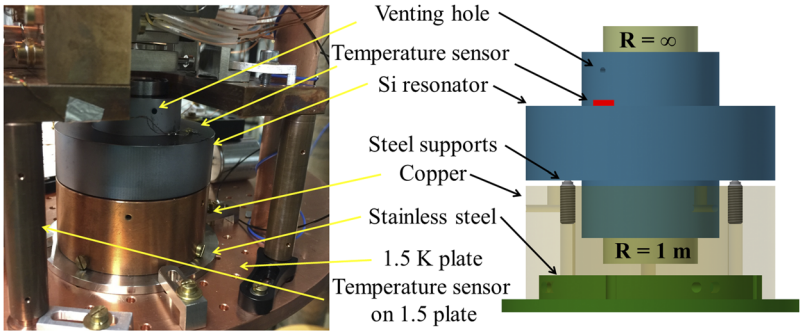

FIG. 4. Cryogenic resonator setup (left) and the corresponding schematic (right).

points. The supports were pressure screws with stainless steel balls at their ends. The balls were cut in half so as to produce a circular surface of 3 mm diameter. To increase the friction between the balls and the resonator, a layer of indium foil was placed between them. In order to reduce the fluctuations of the resonator's temperature caused by the fluctuations of cryostat temperature, we split the support into two parts: a copper cylinder as an intermediate part and a stainless steel base. The latter acts as a thermal low-pass filter, given its reduced thermal conductivity compared to copper. The resonator temperature was measured by using a sensor (cernox) attached to the top surface of the silicon support ring using a cryogenic grease.

B. Cryogenic optical setup

The coupling of the laser light into the resonator and the detection of the resonator response are performed on a cryogenic breadboard with a footprint of 116 × 140 mm^2, shown in Fig. 5. The compact design minimizes the optical path length in order to reduce the effect of unavoidable misalignments upon cooling to cryogenic temperature. Additionally, it incorporates two motorized mirror mounts allowing us to correct for the misalignments.

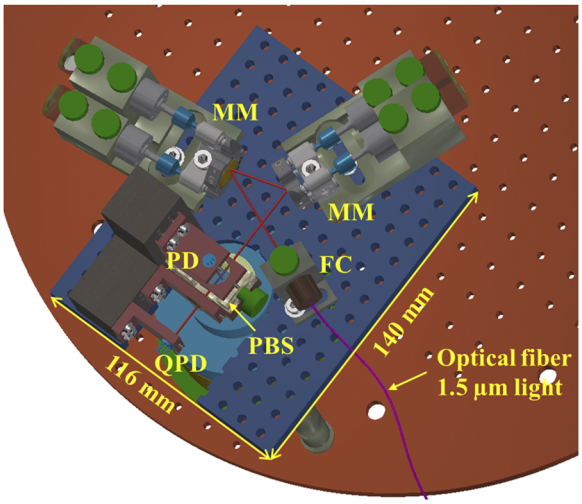

FIG. 5. CAD figure of the cryogenic optical setup. FC, fiber collimator; MM, motorized mirrors; PBS, polarizing beam splitter; QPD, quadrant photodetector; PD, photodetector; and CAM, high-sensitivity infrared InGaAs camera. Red lines indicate free-space paths.

The light of the laser is carried to the breadboard setup using a single-mode polarization-maintaining fiber. The end of the fiber is fixed to the breadboard and coupled out using the fiber collimator (FC). The wave is guided to the resonator by reflecting off two motorized mirrors (MM). Upon reaching the polarizing beam splitter (PBS), a small part of the light is diverted to the quadrant photodetector, marked as QPD, for monitoring the beam position. The remainder is guided to the resonator, passing through a quarter-wave plate (not shown in the schematic). It is partially reflected from the front mirror. The reflected light is detected by using a high-bandwidth photodetector (PD). The signal can be used for a Pound–Drever–Hall-type lock (PDH), not implemented here. The light transmitted by the resonator is split by using a beam splitter. One part is detected by using a photodiode installed below the experimental plate (not shown). The other part exits the cryostat through a window and is used for the identification of the transverse mode excited by the laser. For this purpose, a high-sensitivity room-temperature InGaAs camera is installed outside the cryostat in the beam path.

C. Optical frequency stabilization system and procedures

The concept of the present system is to combine a laser with a good short-term ($\tau \leq 20$ s) frequency stability with a cryogenic resonator whose task is to provide a better frequency stability on medium (>20 s) and long (>1000 s) time scales than possible with a room-temperature reference resonator. Therefore, we use a room-temperature, 10 cm long ULE resonator for the pre-stabilization of the laser's frequency. The pre-stabilized laser then interrogates the TEM_{00} mode of the cryogenic resonator. The overall layout of the optical setup is presented in Fig. 6. It includes components necessary for the characterization of the system performance.

The pre-stabilized laser (optical frequency f_{ULE}) has a linewidth of less than 1 Hz at its output. Part of this light is transferred to the cryogenics lab and into the cryostat via an approximately 50 m long optical fiber. Initially, no active fiber noise cancellation was installed for the path between the pre-stabilized laser and the cryogenic lab. The typical broadening of the linewidth due to fiber noise along this 40 m long path was measured to be 20 Hz. Additional noise is likely introduced by the vibrations inside the cryostat along the

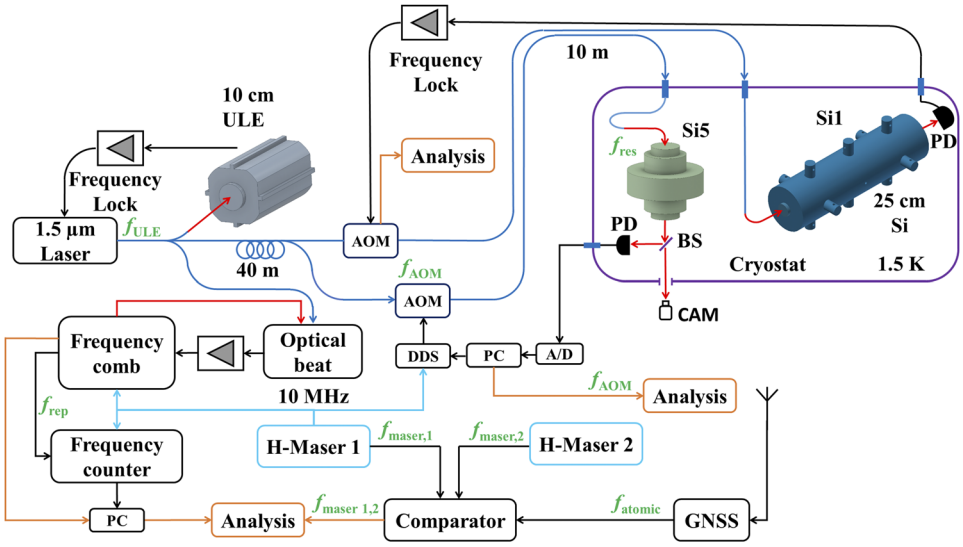

FIG. 6. Overall experimental setup. Red and blue lines indicate free-space and fiber-coupled optical paths, respectively. Black lines represent the electronic paths, and the light blue line is the 10 MHz reference signal from the hydrogen maser. f_{res}, frequency of the cryogenic silicon resonator; f_{ULE}, frequency of the room-temperature ULE resonator; f_{atomic}, frequency of the GNSS satellite signal; $f_{maser,i}$, frequencies of two hydrogen masers; f_{rep}, repetition rate of the frequency comb; f_{AOM}, frequency of the AOM; PC, personal computer; AOM, acousto-optical modulator; DDS, direct digital synthesizer; A/D, analog to digital signal converter; PD, photodiode; BS, beam splitter; and CAM, InGaAs infrared camera for mode detection.

remaining 10 m long fiber but could not be measured independently because no wave reflected back from the resonator or from the end of the fiber could be observed. One part of the pre-stabilized laser light is used for measuring the laser frequency f_{ULE} with a frequency comb referenced to an active hydrogen maser. The maser is continuously compared to a GNSS signal providing a reference frequency f_{atomic}. To improve the sensitivity of the frequency measurements, we reduce the spectral width of the comb lines by phase-locking the comb to the pre-stabilized laser. The repetition rate f_{rep} of the comb is measured with a low-noise frequency counter, and from the data, f_{ULE}/f_{maser} is computed.

Another part of laser light, fiber split in the cryogenic laboratory, is guided to the 25 cm cryogenic ultra-low drift silicon resonator[7] (denoted by "Si1" in some figures) installed on another optical breadboard inside the same cryostat. This resonator is also employed as a reference for determination of the frequency instability of the 5 cm resonator.

We use an acousto-optic modulator (AOM with frequency f_{AOM}) to bridge the gap between the laser frequency f_{ULE} and the frequency of the closest TEM_{00} mode of the silicon resonator, driven by a direct digital synthesizer (DDS) controlled by a personal computer (PC).

To determine the frequency of the resonator, we repeatedly measure the line center frequency. Two techniques have been employed: (1) scanning over the resonance line and (2) alternating interrogation of the half-transmission points of the resonance. Both techniques are compatible with the use of very low light power ($\leq 1\ \mu$W). In addition, they do not require continuous coupling of laser light into the resonator but can be applied, if desired, with a low duty cycle. Together, these features help to reduce permanent or semi-permanent changes in the mirror coatings due to exposure to laser light. Another advantage is the absence of offsets introduced by active optical elements, e.g., residual amplitude modulation introduced by an electro-optical modulator (EOM) or laboratory-temperature-induced variations of the PDH electronics lock point. In the linescan technique, each center frequency determination is carried out by sweeping the frequency of the laser light over the resonance line with an AOM. The light transmitted through the resonator was detected by using the cryogenic detector and the signal sampled by using a 14-bit DAQ card with 40 kS/s. The frequency span was set to twice the linewidth, $2\Delta\nu = 40$ kHz, and the (one-way) scan time was set to 0.7 s. The data of two subsequent scans, upward and downward in frequency, were averaged. These data were subsequently fitted with a Lorentzian function to determine the AOM frequency f_{AOM} corresponding to the resonator's center frequency. This frequency value is thus obtained essentially immediately after each pair of scans. A digital control modifies the scan range settings so as to maintain the resonance frequency in the center of the range. In addition, the value f_{AOM} is stored and used to compute the resonator frequency as $f_{res}/f_{maser} = f_{ULE}/f_{maser} + f_{AOM}/f_{maser}$. In our measurements, the procedure is repeated continuously, but as mentioned, a wait time interval could be inserted if needed.

The detuning technique is realized by periodically shifting the laser light frequency by $\pm\Delta\nu/2$, relative to the resonance frequency f_{res}, to one of the two half-transmission detunings. The signal of the transmission photodiode for $-\Delta\nu/2$ detuning is measured at time step $i-1$ and averaged over a 500 ms time period, yielding the value A_{i-1}. Subsequently, the other half-transmission position is selected and the corresponding amplitude A_i recorded. Then, the frequency correction $\Delta f_{AOM,i} = (\Delta\nu/2)(A_i - A_{i-1})/(A_i + A_{i+1})$ is calculated and applied to the AOM. The absolute frequency of the resonator is computed as in the case of the linescan technique.

IV. CHARACTERIZATION

A. Temperature stability

The temperature stability of the resonator is important since it can affect its medium- and long-term frequency stability through the coefficient of thermal sensitivity of frequency (CTF). Figure 7 compares the temperature instability measured on the resonator and on

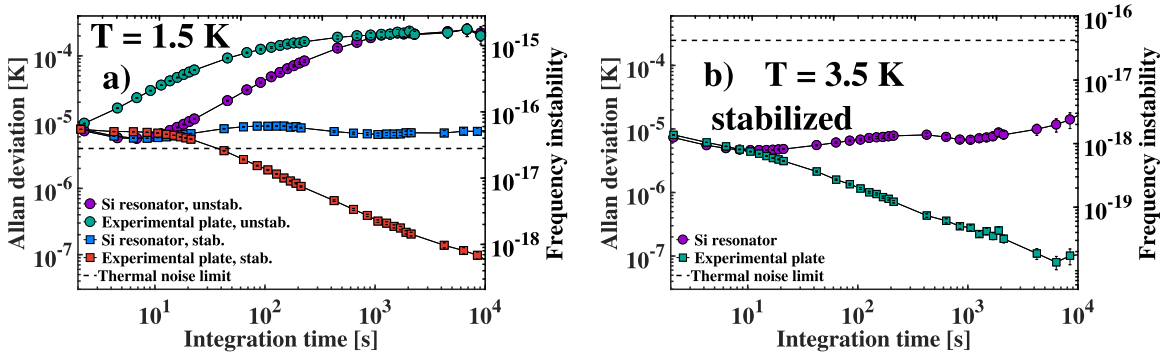

FIG. 7. Temperature instability of the experimental plate, measured with a sensor attached to it in close proximity to the resonator support structure, and of the resonator itself. (a) At 1.5 K, with and without active temperature stabilization, and (b) at 3.5 K, with active stabilization. The right axis in both diagrams shows the resulting fractional frequency instability, computed using the appropriate CTFs.

the base plate, at two operating temperatures, and under two different operating modes. The laser light was blocked during these measurements. The temperature instability is given as a modified Allan deviation and is computed from the temperature time series. At the temperature of 1.5 K, the instability of the free-running resonator temperature is lower than that of the base plate for integration times up to 1000 s. This shows that the baseplate temperature variations are substantially attenuated by the resonator support structure. The smallest temperature instability is 4.5 μK at 6 s integration time. The instability data combined with the thermal expansion coefficient of the resonator at 1.5 K, 7×10^{-12}/K, yield an estimate of the frequency instability of the resonator. This is shown on the right axis of Fig. 7. The instability is above the level of the calculated thermal noise for all integration times. Thus, for operation at 1.5 K, the current support structure would represent a limiting factor for the future resonator performance. An improvement could be realized by introducing a second stage of passive thermal isolation or, as done in this work, by actively stabilizing the temperature of the base plate [see Fig. 7(a)]. This improvement was not necessary for the experimental results presented here.

To operate the setup at 3.5 K, a temperature of particular interest (see below), an active temperature stabilization was implemented. The resulting temperature instability of the resonator is 10 μK or less for all integration times up to 10 000 s. The inferred frequency instability of the resonator, depicted on the right axis, was calculated assuming that the temperature set point has an undesired offset of 0.02 K from the optimum temperature. Such a small deviation is conservative, in view of the accuracy with which the optimum temperature is, in principle, measurable [see Fig. 10(d)]. The absolute value of the CTF is then less than 2×10^{-13}/K. This yields a frequency instability of less than 3×10^{-18}, significantly below the thermal noise limit.

The temperature instability presented in Fig. 7 must be viewed with caution. Variations of laboratory temperature affect the reference voltage in the control electronics of the active temperature stabilization circuit. The voltage variations are interpreted as variations of the cryogenic temperature. This explains the large difference between the instabilities measured by the loop base plate sensor and by the sensor attached to the resonator, as shown in Fig. 7(b). While the in-loop sensor suppresses the influence of the lab temperature variations, the monitor sensor at the resonator does not. Therefore, the temperature instability of the resonator is likely to be equal or below the instability presented in Fig. 7.

B. Resonator properties

After cooling down to 4 K, only a slight optimization of the in-coupling by actuating the mirrors was required. The cooling was then continued down to the operational temperature of 1.5 K. The TEM_{00} resonance was identified and could be routinely interrogated with the pre-stabilized laser. A typical scan is presented in Fig. 8(a). From fits of Lorentzian functions to a series of scans, we find a mean full width at half-maximum of 24.2 ± 0.2 kHz. This corresponds to a finesse of 120 000. The measured in-coupling $(1 - P_{r,on}/P_{r,off})$, where $P_{r,on}$ is the on-resonance reflected power and $P_{r,off}$ is the off-resonance reflected power, was 10%. The mode matching efficiency, determined by characterizing the in-coupling of other transverse modes, was 60%. The fit residuals in this figure deviate clearly from near zero when the laser frequency is tuned to the vicinity of the half-maximum resonator transmission frequency [bottom panel in Fig. 8(a)]. This indicates the presence of frequency fluctuations of the resonator. They are due to the vibrations generated by the cryostat, as can be seen from the fact that the residuals are weaker when the cooler is off [see Fig. 8(b)].

C. Acceleration sensitivity

One of the goals of this work was minimization of the resonator's acceleration sensitivity. The characterization of this property is, therefore, of importance. It is usually done by shaking the resonator along one of the three orthogonal spatial directions and observing the frequency shift of the resonator. However, in our case, the structure of the cryostat prevented us from producing controlled vibrations in desired directions and, thus, made it impossible to measure the vibration sensitivity for the three spatial directions individually. However, we were able to estimate the overall sensitivity of the resonator submitted to the accelerations produced by the cryostat by measuring the variations of the transmission signal caused by the deformations of the resonator.

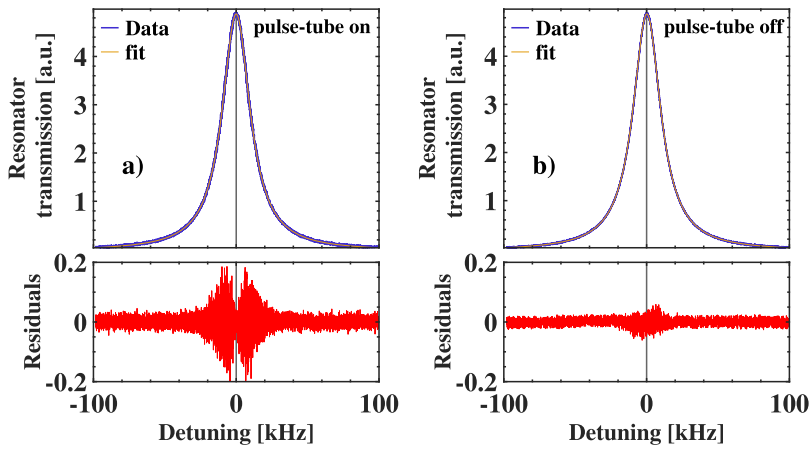

FIG. 8. One-way frequency scans of the pre-stabilized laser frequency over the resonator TEM_{00} mode. Scan duration is 80 s. The signal is the light power transmitted through the resonator. The pulse-tube cooler is on [panel (a)] and off [panel (b)]. The orange lines are Lorentzian fits. Operating temperature: 1.5 K.

An estimate of the sensitivity can be obtained using a side-of-fringe discriminator technique. For this, the laser light is frequency-tuned so that the (time-averaged) transmission signal is half the maximum. Then, the fluctuations of the transmission signal are recorded. Figure 9(a) shows a time trace (orange). For comparison, we also determined the contribution arising from power variations of the laser wave. They were measured with the laser frequency tuned to the maximum transmission of the resonator. Finally, we measured the background noise in the coaxial cable by blocking the laser light. We calculated the rms amplitude deviations corresponding to these

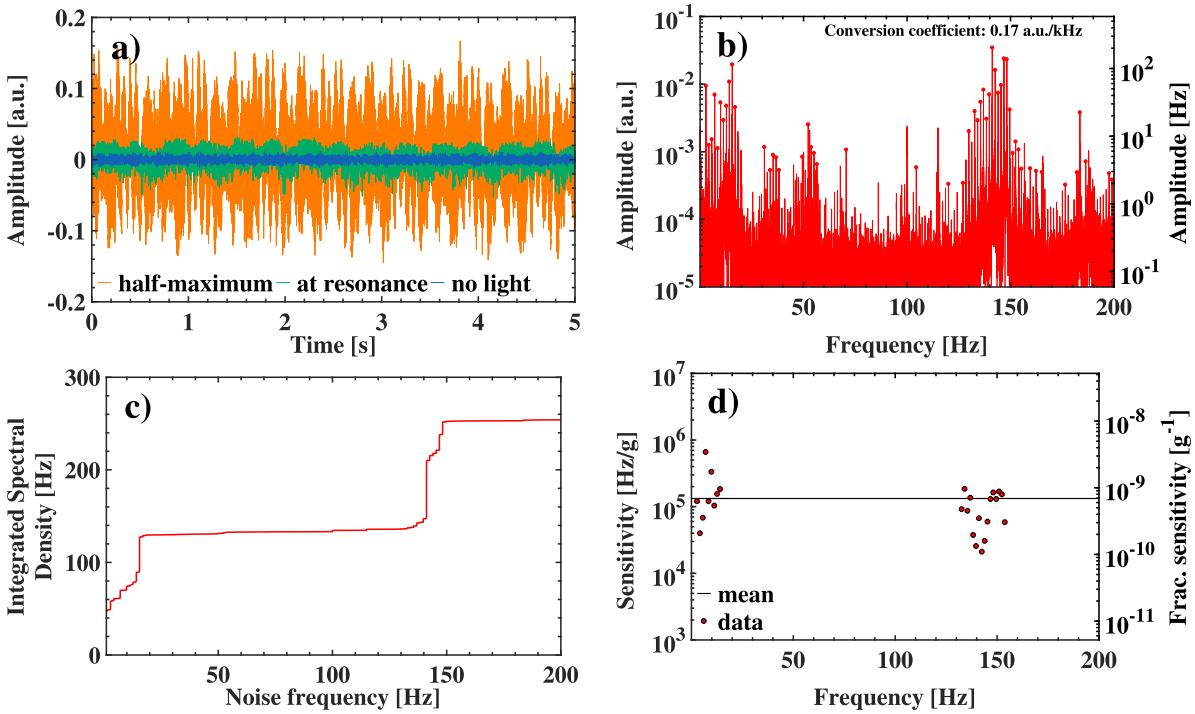

FIG. 9. Determination of the resonator sensitivity to vibrations. (a) Time traces of the cavity transmission signal, with subtracted offset, measured with the laser frequency tuned to the half-transmission of the resonance (orange) and on-resonance (green). The green time trace includes a factor of 1/2 to account for the larger transmitted power. Blue: background signal taken with laser off. (b) Spectrum calculated from the time trace at half-maximum and after subtraction of the spectrum taken with the laser tuned to the resonance and of the noise spectrum. Right y-axis gives the frequency fluctuation level after applying the conversion factor S = 0.17 a.u./kHz (slope of the transmission signal at the half-maximum value). (c) Contribution to the linewidth from vibrations in the frequency region up to 200 Hz. (d) Sensitivity of the resonator to vibrations at different frequencies obtained by division of the spectrum from panel (b) by the spectrum of cryostat accelerations defined as root sum-of-squares of the three individual accelerations. The black line indicates the mean of the shown data points.

three situations, ΔA_S, ΔA_T, and ΔA_N. The rms signal deviation at the half-transmission detuning due to relative frequency fluctuations between laser and resonator, ΔA_{eff}, is obtained after subtraction of $\Delta A_T/2 + \Delta A_N$ from ΔA_S. The correction compared to using only ΔA_S is at the 1% level.

Using ΔA_{eff} together with the slope of resonator transmission at half-maximum, $S = 0.17$ a.u./kHz, and the total acceleration a_{total}, we obtain the acceleration sensitivity $\sigma_{total} = 61.5\ \text{kHz}/g\ (3.2 \times 10^{-10}/g)$.

We obtained the spectrum of frequency fluctuations from the power spectra corresponding to the time traces in Fig. 9(a). It is presented in Fig. 9(b). Conversion into frequency units was done using the transmission signal sensitivity S. Integration of the power spectral density provides an estimate of the linewidth that a laser locked to the resonator would exhibit, assuming that the measured frequency fluctuations are solely due to the resonator length fluctuations. Figure 9(c) shows the integrated frequency noise. The total contribution within the detected bandwidth is 250 Hz. This value is in agreement with the first estimate above. The frequency fluctuations and thus the acceleration noise in the frequency bands [1, 20] Hz and [140, 150] Hz contribute most to the linewidth.

The data in Fig. 9(b) together with the acceleration data in Fig. 1 allow a direct determination of the resonator acceleration sensitivity as a function of frequency by computing their ratio. We show this for the frequency bands mentioned above in Fig. 9(d). The mean

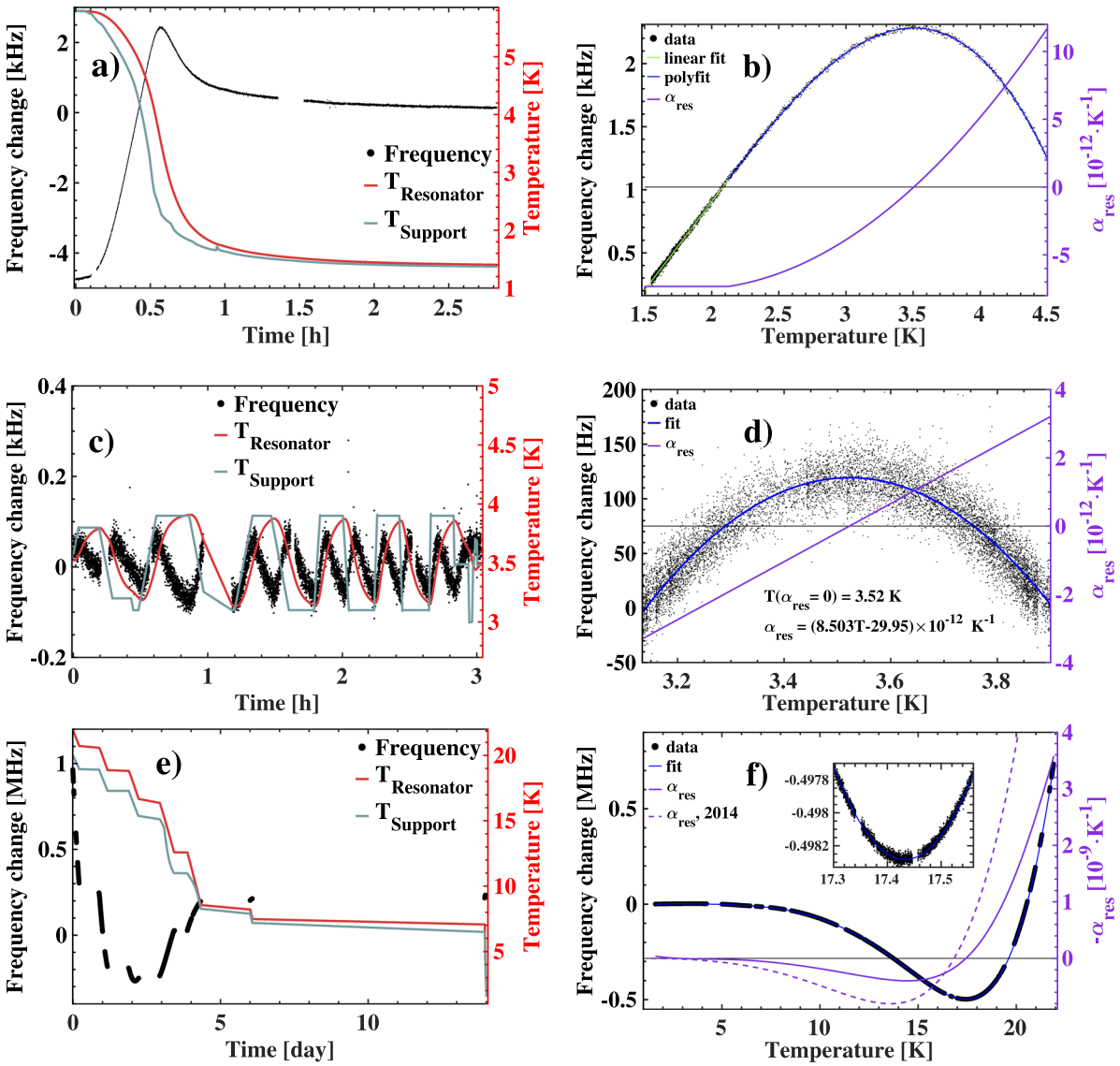

FIG. 10. Measurements of the thermally induced frequency change of the resonator in three temperature ranges: [(a) and (b)] between 1.5 K and 4.5 K, [(c) and (d)] around $T_0 = 3.52$ K (zero CTF), and [(e) and (f)] from 22 K to 1.5 K. The red dashed line in (f) is the result of Ref. 28.

sensitivity is 133 kHz/g ($6.9 \times 10^{-10}/g$). Note that the individual values in the spectrum vary by one order of magnitude around the mean. The largest value is 7×10^2 kHz/g ($5 \times 10^{-9}/g$) at a frequency of 7 Hz. In view of the fact that we cannot separate the contributions of the three spatial components of the acceleration in the transmission signal, our analysis cannot be more precise.

D. Coefficient of thermal sensitivity

The coefficient of thermal sensitivity of frequency (CTF) of our resonator, α_{res}, was determined in the temperature range between 5.5 K and 1.5 K by cooling down or heating up the cryostat over several hours and simultaneously measuring the resonator frequency using the half-transmission detuning technique described above. The raw data of the experiments are presented in Figs. 10(a), 10(c), and 10(e). The total change in resonator frequency from 5.5 K to 1.5 K is 7 kHz. Clearly, the resonator frequency exhibits an extremum at 3.52 K; its CTF vanishes there.

The CTF in the temperature region below 2.12 K was determined by a linear-in-T fit to the data [see Fig. 10(b)]. The resulting CTF is constant; $\alpha_{\mathrm{res}}(T < 2.1\ \mathrm{K}) = -7.33 \times 10^{-12}\ \mathrm{K}^{-1}$ with a fit error smaller than 0.3%. The remaining data were fitted with a cubic polynomial [see Fig. 10(b)]. We find $\alpha_{\mathrm{res}}(2.1\ \mathrm{K} < T < 4.5\ \mathrm{K}) = (2.72(T/\mathrm{K})^2 - 10.0\ (T/\mathrm{K}) + 1.65) \times 10^{-12}\ \mathrm{K}^{-1}$. While the uncertainty of the T^2 coefficient is 2%, it is smaller than 1% for the two remaining coefficients.

In order to determine precisely the temperature of zero CTF, a sinusoidal modulation of the temperature was applied around the mean temperature of $T = 3.5$ K using a heater attached to the experimental plate. The corresponding change in frequency of the resonator is depicted in Fig. 10(c). A quadratic fit was performed [see Fig. 10(d)], yielding a zero CTF temperature $T_0 = 3.52 \pm 0.02$ K with derivative $d\alpha_{\mathrm{res}}/dT = 8.5 \times 10^{-12}/\mathrm{K}^2$. This value is a factor of 40 smaller than at the zero-CTF-temperature 17.4 K, where it is $-3.4 \times 10^{-10}/\mathrm{K}^2$ (see below), and a factor of 2000 lower than at 124.2 K, $1.7 \times 10^{-8}/\mathrm{K}^2$.[26] Assuming that the operating temperature has an undesired offset of 0.02 K from the zero-CTF temperature, the CTF is a factor of 35 smaller than the CTF at 1.5 K.

We also determined the CTF in the extended temperature range between 22 K and T_0 from data obtained during a 15-day-long slow cool-down of the cryostat. The results are presented in Figs. 10(e) and 10(f).

Our results on the CTF for the temperature range below 6 K were confirmed on different occasions: upon heating and cooling of the setup, after prolonged operation (>0.5 year) at 1.5 K and twice immediately after heating of the whole setup to over 100 K. During these measurements, we found a minor variation of the zero CTF temperatures and of the slope at this temperature: ±20 mK and $\pm 1 \times 10^{-12}/\mathrm{K}^2$, respectively.

The CTF results differ significantly from the data published in Ref. 28, which was obtained for a silicon resonator with a different support. While, in that work, the supporting frame was also made of copper, the resonator was held by 10 flexible steel wires that reduced strongly the influence of the thermal expansion of the copper frame. In the present work, the resonator and the copper frame are connected by friction. Thus, a temperature change of the whole setup may conceivably cause a strain $\epsilon = \Delta R/R$ along the radial direction of the resonator due to the much higher expansion coefficient of the copper support, $\alpha_{\mathrm{Cu}}(T = 3.52\ \mathrm{K}) = 2.3 \times 10^{-9}/\mathrm{K}$ (Ref. 35) compared to $\alpha_{\mathrm{Si}}(T = 3.52\ \mathrm{K}) = 2.1 \times 10^{-11}/\mathrm{K}$.[28] This strain is converted into a change in distance between the mirrors $\Delta L/L$ via the material's Poisson's ratio $(\Delta L/L) = -\epsilon\nu$. This hypothesis can be tested by considering the CTF at higher temperatures, where the difference between the CTF of silicon and of copper is larger. For example, at 20 K, $\alpha_{\mathrm{Si}}(T = 20\ \mathrm{K}) = 4 \times 10^{-9}/\mathrm{K}$ (Ref. 28) and $\alpha_{\mathrm{Cu}}(T = 20\ \mathrm{K}) = 0.27 \times 10^{-6}/\mathrm{K}$ (Ref. 36). However, we find a CTF similar to our previous work [see Fig. 10(f)]. The second zero-CTF temperature is $T_0' = 17.4$ K, compared to our earlier $T_0' = 16.8$ K.

Thus, more detailed studies are necessary to determine the precise reason for the zero crossing, including FEM simulations and measurements with different implementations of the contact surfaces between frame and resonator.

V. FREQUENCY STABILITY

We measured the stability of the laser frequency when referenced to the silicon resonator using both techniques outlined above.

A. Medium-term frequency instability

The result of a frequency measurement, allowing us to determine the medium-term frequency instability, and obtained with the linescan technique, is presented in Fig. 11(a). Here, the temperature of the resonator was at 1.47 K and was not actively stabilized. As shown in Fig. 11(a), the frequency stability of the resonator is compromised by the periodic variations of the laboratory temperature. This can be more clearly seen in the FFT spectrum of frequency and temperature time traces, presented in Fig. 11(b). We observe a modulation of frequency with an amplitude of 4 Hz at a time period of 23 min, which is identical to the duration of the laboratory temperature variations. Therefore, we only consider the most stable part of the data, exhibiting the lowest drift, and computed the modified Allan deviation [see Fig. 11(c)]. We find that for integration times up to 1000 s, the laser frequency instability is slightly higher than the beat instability of our two active hydrogen masers and approaches the minimum value of 0.5 Hz (2.5×10^{-15}) at $\tau = 1500$ s. It is possible that this level has a contribution from the temperature variations of the resonator [see Fig. 7(a)].

To verify our results presented in Fig. 11(c), we apply the half-amplitude technique to stabilize the ULE laser light to both the 5 cm resonator and the 25 cm silicon resonator using two independent AOMs (see schematic in Fig. 6). We use the frequency difference between these two resonators for the estimation of frequency instability. This procedure allows us to eliminate fluctuations of the ULE frequency and to avoid an introduction of potentially present additional noise coming from the frequency comb. The result of the measurement is presented in Fig. 12. To determine the frequency instability of the 5 cm resonator, we use the most stable part with a duration of 2 h. The calculated modified Allan deviation of this part is presented in Fig. 12(b).

For integration times $\tau \leqslant 10$ s, the resulting instability is below the instability of the maser. The beat with the ULE resonator shows an instability of 2 Hz (1×10^{-14}) at 1 s integration time.

For integration times from 10 s to 1000 s, the instability of the Si5–Si1 beat follows closely the instability of the maser–maser beat

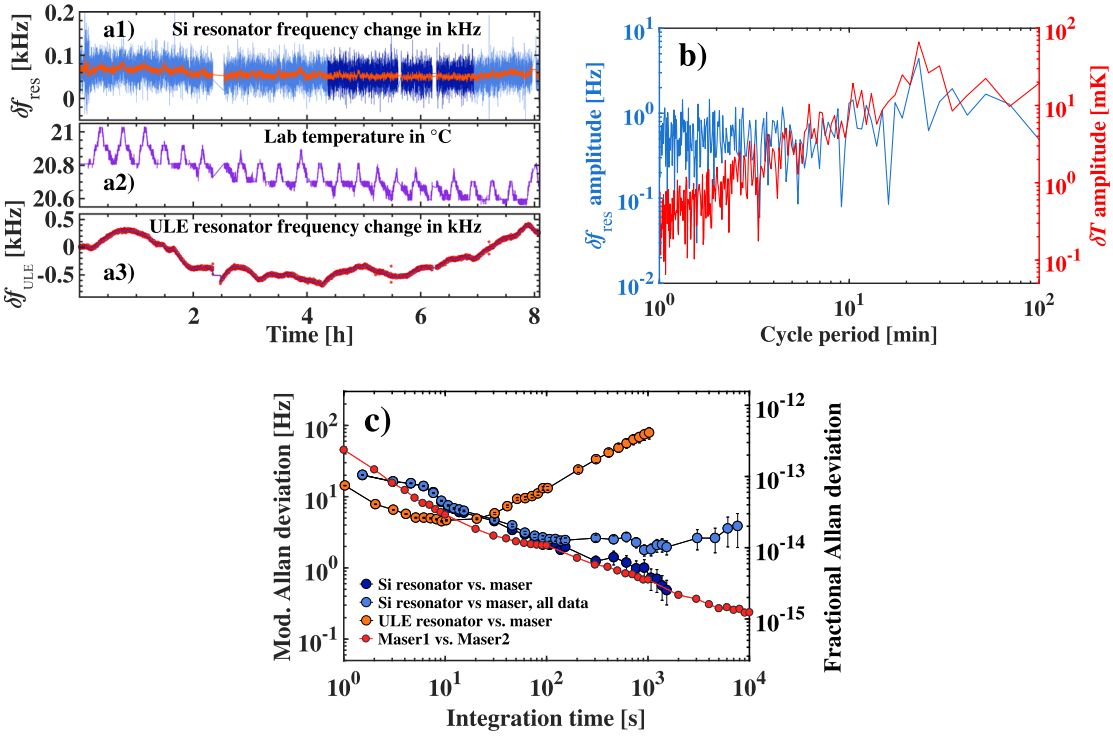

FIG. 11. (a) An 8-h-long laser frequency measurement, with respect to the maser, when the frequency-shifted laser wave tracks the silicon resonator [plot (a1)]. The dark colored interval is used for the calculation of Allan deviation in panel (c). Plots (a2) and (a3) show the temperature of the lab housing the cryostat and the frequency change of the pre-stabilized laser used for interrogation of the silicon resonator, respectively. (b) FFT of the lab temperature and resonator frequency time traces presented in panel (a). (c) Modified Allan deviation of the silicon resonator frequency [whole dataset (light blue markers) and selected part (dark colored blue markers)] and of the pre-stabilized laser (orange markers). No drift was removed. The red points in (c) show the maser instability, determined from a measurement of the frequency difference of two nominally identical masers on a different occasion.

and approaches the minimum instability of 0.8 Hz or 4×10^{-15} at $\tau = 1000$ s integration time. With the assumption that both resonators contribute equally to the instability, we can divide the above result by a factor of $\sqrt{2}$ and obtain 0.6 Hz (3×10^{-15}) at $\tau = 1000$ s integration time.

VI. LONG-TERM FREQUENCY DRIFT

The long-term ($\tau > 10\,000$ s) frequency drift of the resonator is mainly determined by the length changes of the spacer due to the relaxation processes in the crystal lattice and photochemical changes

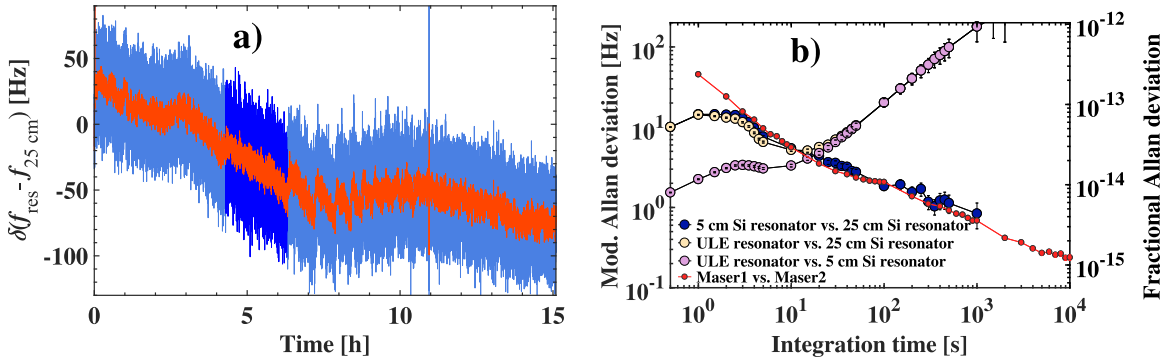

FIG. 12. (a) A 15-h-long measurement of the frequency of the 5 cm silicon resonator relative to the frequency of the 25 cm silicon resonator. The 2-h-long dark colored interval is used for the calculation of Allan deviation. (b) Modified Allan deviation of the frequency difference [selected part in panel (a)] between the silicon resonator and the 25 cm silicon resonator (dark blue markers). A drift of 5 mHz/s was removed. Purple and yellow markers represent the frequency instability of the silicon resonator and the 25 cm silicon resonator relative to the ULE resonator, respectively, measured simultaneously. Red points show the maser instability, determined from a measurement of the frequency difference of two nominally identical masers 1 and 2 on a different occasion.

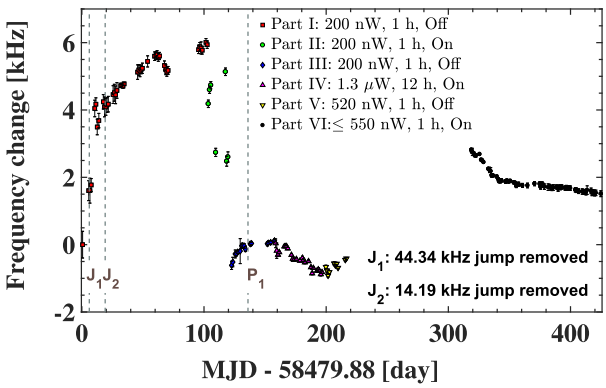

FIG. 13. Frequency change of the resonator measured over a time span of 425 days. Between day 217 and 318, no data were recorded because the temperature of the resonator was changed to measure the coefficient of thermal sensitivity. J_1 and J_2 mark two frequency jumps that occurred during the measurement; P_1 marks the time when we changed from the line scan technique to the half-amplitude detuning technique. The legend sates for each part: the incident optical power of the laser during the measurements, the measurement duration per working day, and whether the laser light was on or off in-between measurements on subsequent days.

in the mirror coatings. The latter are found to depend on the cumulative irradiation duration by the laser and the applied laser power. In our previous work with horizontally oriented silicon resonators supported as described above, we observed an exponential relaxation of the frequency and a positive drift rate after a long time.[7] In those measurements, we interrogated the resonator with a pre-stabilized laser wave of 1 μW power for a duration of 1 h each day and blocked the laser light for the remaining 23 h.

The long-term frequency drift rate of the 5 cm resonator was determined by repeatedly scanning over its resonance line with the pre-stabilized laser light over a time period of 425 days, starting at a day zero (MJD 58479.88), when the system reached the temperature of 1.5 K. The results are presented in Fig. 13. We subtracted two frequency jumps, marked as J_1 and J_2. They were probably caused by spontaneous relaxation processes in the crystalline spacer and/or in the substrates.

In order to gain insight into the drift behavior, we varied the incident laser power. It was kept at 200 nW for all measurements up to day 154. From the following day and up to day 197, the optical power was increased to the level of 1.3 μW. It was reduced again to 520 nW for the days up to day 216. From day 320 to day 425, the power was subsequently reduced from 550 nW to 100 nW. On five days between day 102 and day 122, we optimized the in-coupling of the laser light to the lower mirror of the resonator for the installation of the Pound–Drever–Hall setup attached to the vacuum enclosure of the cryostat. The incident light power on these occasions was on the order of 1 mW.

To determine the frequency of the resonator, we used the lines-can technique from day 1 to day 137. After this day, marked as P_1 in the diagram, we changed to the half-transmission technique. The daily interrogation duration was ~1 h on all working days except for two time periods from day 159 to day 197 and from day 320 to day

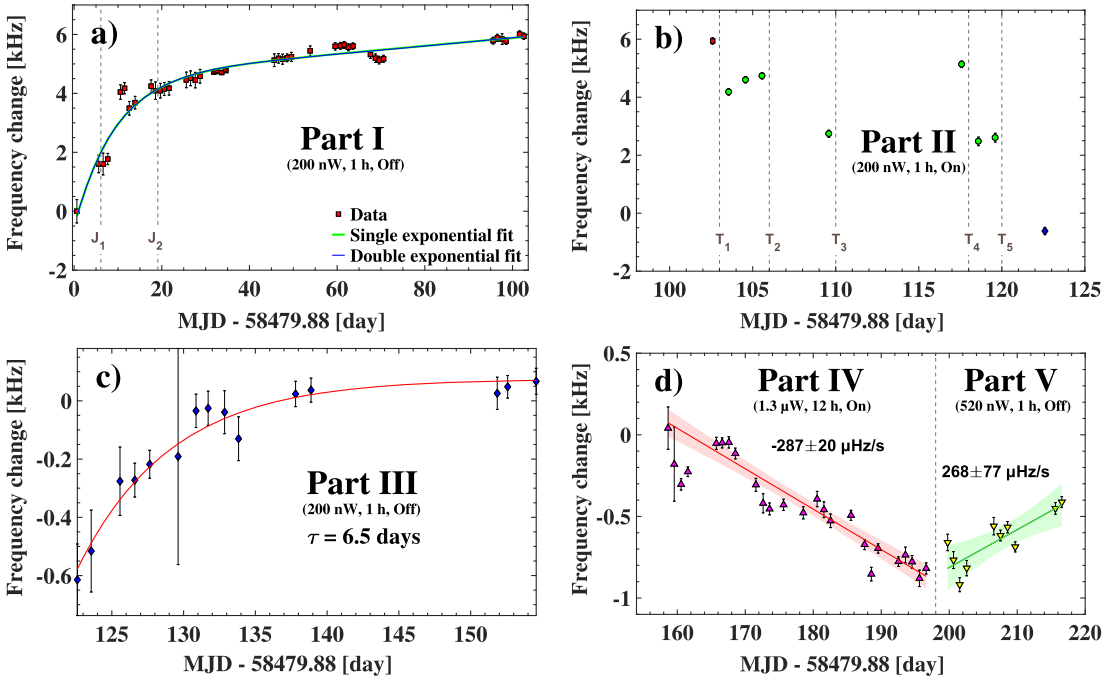

FIG. 14. Zoomed-in views of different intervals of the long-term frequency measurement campaign: (a) part I; (b) part II: T_1–T_5 mark the times when a separate 1 mW free-space laser beam was coupled to the resonator on the bottom side and in addition, regular 1 h-long daily frequency measurements were performed with an incident optical power of 200 nW; (c) part III: subsequent relaxation (interrogation at low power); and (d) parts IV and V. Linear fits and corresponding drift rates are shown.

425 when it was increased to 12 h and 8 h on average, respectively. The laser light was blocked between the measurements from day 1 to day 158. For the two mentioned time periods from day 159 to day 197 and from day 320 to day 425, the laser light was not at resonance when no measurements were performed (i.e., for 12 h per working day and 24 h on the weekend days), but it was still incident on the front mirror of the resonator.

Starting immediately after cool-down, we observed a relaxation of the resonator frequency with a measured total frequency change of 6 kHz over the first 100 days. We denote this measurement period as part I in Fig. 14. The frequency change is positive, meaning that the distance between the two mirrors is decreasing with time. The rate of frequency change is not constant over time.

At the end of part I, the drift rate was 9.7×10^{-19}/s. This value is a factor of 3 higher than the drift measured on a resonator with comparable dimensions by Ref. 24 and a factor of 70 higher compared to our previous result obtained with a 25 cm long silicon resonator.[7] However, this latter drift was measured after almost a year-long continuous operation at 1.5 K. The drift after the first 100 days was almost identical to the current result, 1×10^{-18}/s.

During part II [Fig. 13(b)], on five occasions with a duration of ~4 h each (marked as T_i in this figure), a laser beam with 1 mW optical power was coupled to the resonator mode for most of that time through a cryostat window and to the bottom end of the resonator. Frequency measurements during this time interval (performed as usual) display negative frequency changes. After each optimization of the PDH setup, there is a frequency jump on the order of −2 kHz to −3 kHz. These jumps have a different sign, compared to two jumps J_1 and J_2 [see Fig. 13(a)], suggesting that the two underlying processes are different in nature.

After completion of the optimization, we observe an exponential relaxation process with $\tau = 6.6$ days over the next month [part III, see Fig. 14(c)]. As shown in Fig. 13, the resonator frequency did not return to the original value, implying that the changes induced by high-power irradiation were permanent.

Figure 14(d) displays the next two parts of the measurement campaign, parts IV and V. The frequency drift rate changes from negative to positive after the reduction in power from 1.3 μW to 520 nW and interrogation time from 12 h to 1 h.

During part VI, we performed a systematic study of the frequency drift dependence on the optical laser power, where we continuously decreased the level of optical power from 550 nW to 100 nW [see Fig. 15(a)]. To simulate the realistic conditions of a day-to-day operation of the resonator, we increased the duty cycle to an average duration of 8 h per day [see Fig. 15(b)]. To exclude possible thermal influences, we actively stabilized the temperature at 1.4 K during this time period. In line with the measurements in parts VI and V, we observe a decrease in the frequency drift with the reduction in optical power. The lowest drift of -48.7 ± 3.5 μHz/s (-2.6×10^{-19}/s) is measured at an optical power of 100 nW.

Our observation of negative and positive drift is in contrast to the results presented by Robinson *et al.*,[24] where the drift was always negative, regardless of the optical power. This discrepancy may be due to the differences in the mirror coatings, as well as differences in purity and internal stress of the mirror substrate material. Another factor could be the length of time that the resonator was operated at cryogenic temperature.

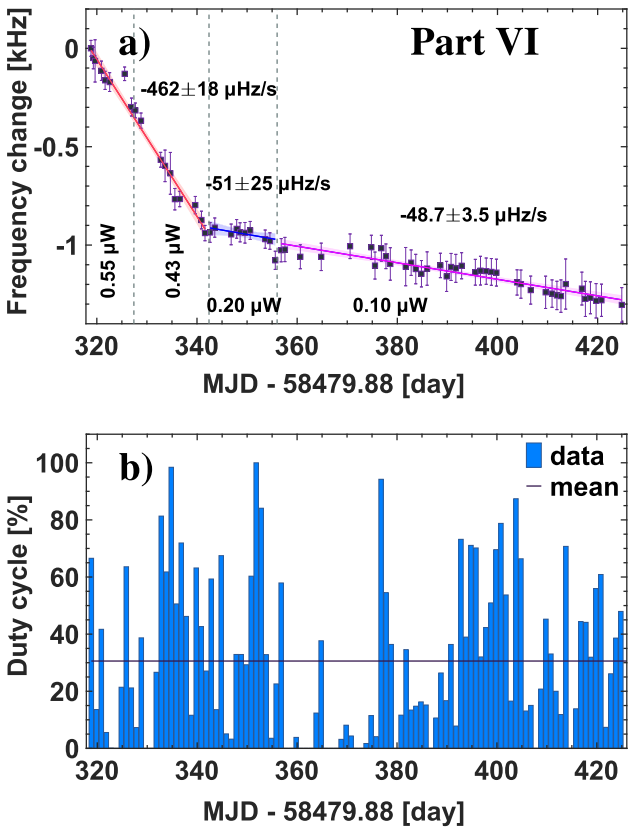

FIG. 15. (a) Frequency change of the resonator measured over a time span of 105 days as a function of optical power. (b) The duty cycle of the resonator interrogation in percent per day.

VII. CONCLUSION

We have developed a relatively simple system for the stabilization of the frequency of a laser on short- and medium-time intervals with the goal of reaching a performance and a reliability comparable to a hydrogen maser. The system is based on a 5 cm long, vertically oriented, silicon resonator operated at cryogenic temperature. The system was characterized in detail. First, it is capable of continuous operation. Except for realignment after initial cool-down, no significant intervention is necessary when the resonator is operated either at 1.5 K or at 3.5 K. Here, we reported on over one year of data and the characterization of the resonator's properties.

Second, the resonator vibration sensitivity was measured to be $3 \times 10^{-10}/g$ in fractional terms. Together with vibrations produced by the cryostat, we expect this to be the limiting factor for the short-term frequency instability of the resonator, which is equal to 1×10^{-14} at 1 s.

At long integration times (1500 s), the instability is not more than 2.5×10^{-15}, similar to the instability of the reference hydrogen maser.

The long-term frequency drift rate was found to depend on the power of the interrogating laser wave and on the duty cycle of the interrogation. Our results, together with previous studies,[7,24,27]

indicate that in the limit of very low interrogation laser power and very low duty cycle, the drift rate becomes extremely small.

By varying these parameters, we could change the amplitude and sign of the drift rate. The drift rate can be rather precisely modified, and this feature might, in the future, be used to produce a nearly drift-free frequency reference.

We also characterized the temperature dependence of the resonator frequency. We found two temperature values at which the frequency has zero sensitivity with respect to temperature: 3.5 K and 17.4 K. While the latter value is well known, the former is new. The much smaller temperature derivative of the thermal frequency sensitivity at 3.5 K is highly advantageous, allowing us to suppress temperature-induced frequency instability below the Brownian noise for all integration times. Moreover, the temperature value 3.5 K is sufficiently high that it may be reached in cryostats not equipped with a Joule–Thomson stage. This implies reduced complexity and purchase and maintenance costs. Detailed studies are necessary to determine the origin of this promising property.

To improve the performance of our system, a cryostat that decouples vibrations of the cooler from the resonator is required. Such cryostats are commercially available. We also note that the linewidth of the resonator (24.2 kHz) could be lowered by replacing the current mirrors with mirrors having lower loss; this could also improve the performance of the system. In the future, a more precise characterization of the instability could be done using as reference a high-performance atomic standard (Cs clock or optical atomic clock).

ACKNOWLEDGMENTS

We are thankful to M. G. Hansen for his help with the operation of the frequency comb and A. Yu. Nevsky for stimulating discussions.

E.W. acknowledges a fellowship from the Professor W. Behmenburg-Schenkung. This work was performed in the framework of project SCHI 431/21-1 of the Deutsche Forschungsgemeinschaft.

REFERENCES

[1] A. D. Ludlow, M. M. Boyd, J. Ye, E. Peik, and P. O. Schmidt, "Optical atomic clocks," Rev. Mod. Phys. **87**, 637 (2015).
[2] A. Derevianko and H. Katori, "Colloquium: Physics of optical lattice clocks," Rev. Mod. Phys. **83**, 331 (2011).
[3] N. Poli, C. W. Oates, P. Gill, and G. M. Tino, "Optical atomic clocks," Riv. Nuovo Cimento **36**, 555 (2013).
[4] C. M. Will, "The Confrontation between General Relativity and Experiment," Living Rev. Relativ. **17**, 4 (2014).
[5] R. X. Adhikari, "Gravitational radiation detection with laser interferometry," Rev. Mod. Phys. **86**, 121 (2014).
[6] C. Braxmaier, H. Müller, O. Pradl, J. Mlynek, A. Peters, and S. Schiller, "Test of relativity using a cryogenic optical resonator," Phys. Rev. Lett. **88**, 010401 (2002).
[7] E. Wiens, A. Y. Nevsky, and S. Schiller, "Resonator with ultrahigh length stability as a probe for equivalence-principle-violating physics," Phys. Rev. Lett. **117**, 271102 (2016).
[8] Q. Chen, E. Magoulakis, and S. Schiller, "High-sensitivity crossed-resonator laser apparatus for improved tests of Lorentz invariance and of space-time fluctuations," Phys. Rev. D **93**, 022003 (2016).
[9] M. E. Tobar, P. Wolf, S. Bize, G. Santarelli, and V. Flambaum, "Testing local Lorentz and position invariance and variation of fundamental constants by searching the derivative of the comparison frequency between a cryogenic sapphire oscillator and hydrogen maser," Phys. Rev. D **81**, 022003 (2010).
[10] C. Eisele, A. Nevsky, and S. Schiller, "A laboratory test of the isotropy of light propagation at the 10^{-17} level," Phys. Rev. Lett. **103**, 090401 (2009).
[11] M. Nagel, S. R. Parker, E. V. Kovalchuk, P. L. Stanwix, J. G. Hartnett, E. N. Ivanov, A. Peters, and M. E. Tobar, "Direct terrestrial test of Lorentz symmetry in electrodynamics to 10^{-18}," Nat. Commun. **6**, 8174 (2015).
[12] A. Takahashi, "Long-term dimensional stability of a line scale made of low thermal expansion ceramic nexcera," Meas. Sci. Technol. **23**, 035001 (2012).
[13] K. Hosaka, H. Inaba, D. Akamatsu, M. Yasuda, J. Sugawara, A. Onae, and F.-L. Hong, "A Fabry-Perot etalon with an ultralow expansion ceramic," Jpn. J. Appl. Phys., Part 1 **52**, 032402 (2013).
[14] I. Ito, A. Silva, T. Nakamura, and Y. Kobayashi, "Stable cw laser based on low thermal expansion ceramic cavity with 4.9 mHz/s frequency drift," Opt. Express **25**, 26020 (2017).
[15] K. Numata, A. Kemery, and J. Camp, "Thermal-noise limit in the frequency stabilization of lasers with rigid cavities," Phys. Rev. Lett. **93**, 250602 (2004).
[16] A. D. Ludlow, X. Huang, M. Notcutt, T. Zanon-Willette, S. M. Foreman, M. M. Boyd, S. Blatt, and J. Ye, "Compact, thermal-noise-limited optical cavity for diode laser stabilization at 1×10^{-15}," Opt. Lett. **32**, 641 (2007).
[17] S. A. Webster, M. Oxborrow, S. Pugla, J. Millo, and P. Gill, "Thermal-noise-limited optical cavity," Phys. Rev. A **77**, 033847 (2008).
[18] Q.-F. Chen, A. Nevsky, M. Cardace, S. Schiller, T. Legero, S. Häfner, A. Uhde, and U. Sterr, "A compact, robust, and transportable ultra-stable laser with a fractional frequency instability of 1×10^{-15}," Rev. Sci. Instrum. **85**, 113107 (2014).
[19] D. Świerad, S. Häfner, S. Vogt, B. Venon, D. Holleville, S. Bize, A. Kulosa, S. Bode, Y. Singh, K. Bongs, E. M. Rasel, J. Lodewyck, R. Le Targat, C. Lisdat, and U. Sterr, "Ultra-stable clock laser system development towards space applications," Sci. Rep. **6**, 33973 (2016).
[20] J. Davila-Rodriguez, F. N. Baynes, A. D. Ludlow, T. M. Fortier, H. Leopardi, S. A. Diddams, and F. Quinlan, "Compact, thermal-noise-limited reference cavity for ultra-low-noise microwave generation," Opt. Lett. **42**, 1277 (2017).
[21] S. Häfner, S. Falke, C. Grebing, S. Vogt, T. Legero, M. Merimaa, C. Lisdat, and U. Sterr, "8×10^{17} fractional laser frequency instability with a long room-temperature cavity," Opt. Lett. **40**, 2112–2115 (2015).
[22] D. G. Matei, T. Legero, S. Häfner, C. Grebing, R. Weyrich, W. Zhang, L. Sonderhouse, J. M. Robinson, J. Ye, F. Riehle, and U. Sterr, "1.5 μm lasers with sub-10 mHz linewidth," Phys. Rev. Lett. **118**, 263202 (2017).
[23] W. Zhang, J. M. Robinson, L. Sonderhouse, E. Oelker, C. Benko, J. L. Hall, T. Legero, D. G. Matei, F. Riehle, U. Sterr, and J. Ye, "Ultrastable silicon cavity in a continuously operating closed-cycle cryostat at 4 K," Phys. Rev. Lett. **119**, 243601 (2017).
[24] J. M. Robinson, E. Oelker, W. R. Milner, W. Zhang, T. Legero, D. G. Matei, F. Riehle, U. Sterr, and J. Ye, "Crystalline optical cavity at 4 K with thermal-noise-limited instability and ultralow drift," Optica **6**, 240–243 (2019).
[25] S. Seel, R. Storz, G. Ruoso, J. Mlynek, and S. Schiller, "Cryogenic optical resonators: A new tool for laser frequency stabilization at the 1 Hz level," Phys. Rev. Lett. **78**, 4741 (1997).
[26] T. Kessler, C. Hagemann, C. Grebing, T. Legero, U. Sterr, F. Riehle, M. J. Martin, L. Chen, and J. Ye, "A sub-40-mHz-linewidth laser based on a silicon single-crystal optical cavity," Nat. Photonics **6**, 687 (2012).
[27] C. Hagemann, C. Grebing, C. Lisdat, S. Falke, T. Legero, U. Sterr, F. Riehle, M. Martin, and J. Ye, "Ultra-stable laser with average fractional frequency drift rate below 5×10^{-19}/s," Opt. Lett. **39**, 5102 (2014).
[28] E. Wiens, Q. Chen, I. Ernsting, H. Luckmann, A. Y. Nevsky, U. Rosowski, and S. Schiller, "A silicon single-crystal cryogenic optical resonator," Opt. Lett. **39**, 3242 (2014).
[29] H. Müller, C. Braxmaier, S. Herrmann, O. Pradl, C. Lämmerzahl, J. Mlynek, S. Schiller, and A. Peters, "Testing the foundation of relativity using cryogenic optical resonators," Int. J. Mod. Phys. D **11**, 1101 (2002).

[30]J. J. Hall, "Electronic effects in the elastic constants of n-type silicon," Phys. Rev. **161**, 756 (1967).
[31]D. G. Matei, T. Legero, C. Grebing, S. Häfner, C. Lisdat, R. Weyrich, W. Zhang, L. Sonderhouse, J. M. Robinson, F. Riehle, J. Ye, and U. Sterr, "A second generation of low thermal noise cryogenic silicon resonators," J. Phys.: Conf. Ser. **723**, 012031 (2016).
[32]L. Zhang, R. Barrett, P. Cloetens, C. Detlefs, and M. Sanchez del Rio, "Anisotropic elasticity of silicon and its application to the modelling of x-ray optics," J. Synchrotron Radiat. **21**, 507 (2014).
[33]R. Nawrodt, A. Zimmer, T. Koettig, C. Schwarz, D. Heinert, M. Hudl, R. Neubert, M. Thürk, S. Nietzsche, W. Vodel, P. Seidel, and A. Tünnermann, "High mechanical Q-factor measurements on silicon bulk samples," J. Phys.: Conf. Ser. **122**, 012008 (2008).
[34]M. Granata, K. Craig, G. Cagnoli, C. Carcy, W. Cunningham, J. Degallaix, R. Flaminio, D. Forest, M. Hart, J.-S. Hennig, J. Hough, I. MacLaren, I. W. Martin, C. Michel, N. Morgado, S. Otmani, L. Pinard, and S. Rowan, "Cryogenic measurements of mechanical loss of high-reflectivity coating and estimation of thermal noise," Opt. Lett. **38**, 5268 (2013).
[35]K. O. McLean, "Low temperature thermal expansion of copper, silver, gold and aluminum," Ph.D. thesis, Iowa State University, 1969.
[36]*Materials at Low Temperatures*, edited by R. P. Reed and A. F. Clark (American Society for Metals, 1983).